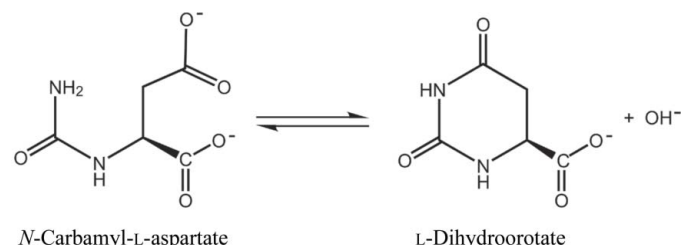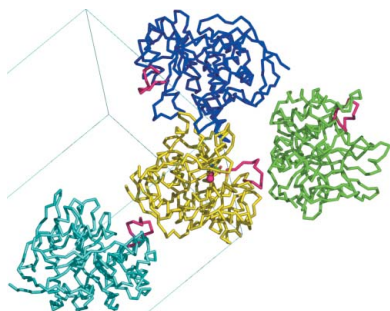# Structure of the T109S mutant of *Escherichia coli* dihydroorotase complexed with the inhibitor 5-fluoroorotate: catalytic activity is reflected by the crystal form

**Mihwa Lee,[a] Megan J. Maher[b] and J. Mitchell Guss[a]***

[a]School of Molecular and Microbial Biosciences (G08), University of Sydney, NSW 2006, Australia, and [b]Division of Biomolecular Sciences, Imperial College, London SW7 2ZA, England

Correspondence e-mail: m.guss@mmb.usyd.edu.au

Crystals of a single-point mutant (T109S) of *Escherichia coli* dihydroorotase (DHOase) with diminished activity grown in the presence of L-dihydroorotate (L-DHO) are tetragonal, with a monomer in the asymmetric unit. These crystals are extremely unstable and disintegrate shortly after formation, which is followed by the growth of orthorhombic crystals from the remnants of the tetragonal crystals or at new nucleation sites. Orthorhombic crystals, for which a structure has previously been reported [Thoden *et al.* (2001), *Biochemistry*, **40**, 6989–6997; Lee *et al.* (2005), *J. Mol. Biol.* **348**, 523–533], contain a dimer of DHOase in the asymmetric unit; the active site of one monomer contains the substrate *N*-carbamyl-L-aspartate (L-CA-asp) and the active site of the other monomer contains the product of the reaction, L-DHO. In the subunit with L-DHO in the active site, a surface loop (residues 105–115) is 'open'. In the other subunit, with L-CA-asp in the active site, the loop folds inwards, forming specific hydrogen bonds from the loop to the L-CA-asp. The tetragonal crystal form can be stabilized by crystallization in the presence of the inhibitor 5-fluoroorotate (FOA), a product (L-DHO) mimic. Crystals of the complex of T109S DHOase with FOA are tetragonal, space group $P4_12_12$, with unit-cell parameters $a = b = 72.6$, $c = 176.1$ Å. The structure has been refined to $R$ and $R_{free}$ values of 0.218 and 0.257, despite severe anisotropy of the diffraction. In this structure, the flexible loops are both in the 'open' conformation, which is consistent with FOA, like L-DHO, binding at both sites. The behaviour of the T109S mutant crystals of DHOase in the presence of L-DHO is explained by initial binding of L-DHO to both subunits, followed by slow conversion to L-CA-asp, with consequent movement of the flexible loop and dissolution of the crystals. Orthorhombic crystals are then able to grow in the presence of L-DHO and L-CA-asp.

## 1. Introduction

Dihydroorotase (DHOase; EC 3.5.2.3) is a zinc metalloenzyme that catalyzes the reversible cyclization of *N*-carbamyl-L-aspartate (L-CA-asp) to L-dihydroorotate (L-DHO) in the third step of the *de novo* pyrimidine-synthetic pathway (Fig. 1). The reversible reaction catalyzed by DHOase is pH-dependent (Christopherson & Jones, 1979; Porter *et al.*, 2004). The biosynthetic direction (cyclization of L-CA-asp to L-DHO) is favoured at lower pH, while the degradative rate (L-DHO to L-CA-asp) is maximal at alkaline pH.

DHOase belongs to the amidohydrolase superfamily, which comprises a variety of hydrolytic enzymes of the $(\beta/\alpha)_8$-barrel (or TIM-barrel) fold (Holm & Sander, 1997). The active sites of enzymes belonging to the amidohydrolase superfamily have five highly

**Figure 1**
Cyclization of *N*-carbamyl-L-aspartate (L-CA-asp) to L-dihydroorotate (L-DHO).

conserved metal-binding residues, usually four histidine residues and one aspartate residue, and one or two metal ions. A common feature of the enzyme mechanism is the utilization of an activated water or hydroxide molecule bound to the metal ion(s) at the catalytic centre.

A phylogenetic analysis of the amino-acid sequences of DHOase reveals that the enzyme can be divided into two major classes that have diverged from a common ancestor of the amidohydrolase superfamily (Fields *et al.*, 1999). Type I DHOases are the more ancient form and are found in all domains of life; they include the DHOase domain of mammalian CAD and monofunctional DHOases found in Gram-positive bacteria, including *Bacillus*, *Lactobacillus* and *Streptococcus*. Mammalian CAD is a trifunctional enzyme consisting of the first three enzyme activities in the pyrimidine-synthetic pathway: carbamyl phosphate synthetase (CPSase), aspartate transcarbamylase (ATCase) and DHOase (Simmer *et al.*, 1990; Williams *et al.*, 1990). Type II DHOases are smaller (~38 kDa compared with ~45 kDa for the type I DHOases) monofunctional enzymes that are found predominantly in Gram-negative bacteria (*e.g. Escherichia coli*) and have a low level of sequence identity to their type I counterparts.

To date, the structures of two DHOases, those from *E. coli* and *Aquiflex aeolicus*, have been reported [PDB codes 1j79 and 1xge (Thoden *et al.*, 2001; Lee *et al.*, 2005) and 1xrt and 1xrf (Martin *et al.*, 2005)]. *E. coli* DHOase is a monofunctional and homodimeric enzyme. Although the *E. coli* DHOase has been reported to contain one catalytic zinc per monomer (Brown & Collins, 1991; Washabaugh & Collins, 1984, 1986), the structure clearly showed that the active site contains a binuclear centre with a carboxylated lysine as one of the bridging ligands. In the original structure determination of *E. coli* DHOase, the crystals grown in the presence of racemic substrate, D,L-CA-asp, were orthorhombic with a dimer in the asymmetric unit. Interestingly, one subunit contained bound L-DHO and the other contained L-CA-asp (Thoden *et al.*, 2001).

In our subsequent study of *E. coli* DHOase, we found two different conformations of a surface loop comprised of residues 105–115 (Lee *et al.*, 2005). We also found asymmetry between the active sites in the dimer, with the product L-DHO in one subunit and the substrate L-CA-asp in the other, despite the fact that we used the product rather than the substrate to form the complex. However, we were able to resolve the positions of residues (109–112 from chain *B*) that were missing from the original structure and to observe two conformations of the surface loop (residues 105–115). The ability to resolve the surface loops in our structure was attributed to the use of optically pure L-DHO rather than racemic D,L-CA-asp in the crystallization medium. The loop asymmetry mirrored that of the active-site contents of the two subunits. In the substrate-bound subunit the surface loop (residues 105–115) reaches in towards the active site and makes two hydrogen-bonding interactions with the bound substrate molecule *via* two threonine residues (Thr109 and Thr110; 'loop-in'), whereas the loop forms part of the surface of the protein in the product-bound subunit ('loop-out'). Subsequent enzyme kinetics at low concentrations of L-DHO in the reverse degradative reaction showed positive cooperativity between the subunits.

Conformational changes during enzyme catalysis have been observed in many different enzymes and appear to be a general feature of enzymatic mechanisms (Gutteridge & Thornton, 2004; Hammes, 2002; Kempner, 1993). One of the movements involved in enzyme catalysis is the rearrangement of loops that constitute active-site lids. The conformations of these loops are tightly coupled to the catalytic state of the enzyme. In general, these movements are characterized by a closing of the active site, with the surface-loop regions moving in towards the active site of the protein, closing over the bound substrate. Catalysis takes place in the closed form and the enzyme opens again to release the product. This motion from open to closed is thought to fulfil a number of roles in enzyme reactions: (i) arrangement of the catalytic residues into the correct orientation for catalysis and/or restriction of the conformational freedom of the substrate, (ii) prevention of the escape of reaction intermediates before the reaction has completed and (iii) restriction of the entry of water and its subsequent reaction with unstable reaction intermediates.

To probe the role of the surface-loop movement of *E. coli* DHOase in catalysis, we generated a series of single-point mutants. The two threonine residues (Thr109 and Thr110) that interact with the bound substrate L-CA-asp in the active site of the wild-type enzyme were mutated to a number of different amino acids. The mutation of these residues produced enzymes with lower catalytic activities (unpublished work). In this paper, we report the crystal structure of one of the single-point mutants (T109S) of *E. coli* DHOase in complex with a product mimic, FOA (Fig. 2). We also discuss the behaviour of crystals of the mutant enzyme in the presence of L-DHO, which reveals a macroscopic effect of the loop movement on catalysis and crystallization.

## 2. Materials and methods

### 2.1. Generation of T109S mutant DHOase

Mutation of Thr109 to Ser in *E. coli* DHOase was generated using the QuikChange site-directed mutagenesis kit (Stratagene, La Jolla, CA, USA) with forward primer 5′-CCGGCAAACGCA**AGC**CAC-ACTAACTCCAGCCA-3′ and reverse primer 5′-TGGCTGGAGT-TAGT**GCT**TGCGTTTGCCGG-3′. The wild-type DHOase in the pBS+ vector was used as a template and the mutations were confirmed by determination of the nucleotide sequences of the whole gene. *E. coli* strain X7014a, which lacks a gene for dihydroorotase, was obtained from the Yale *E. coli* Genetic Stock Center (Yale University, New Haven, CT, USA) and used for expression and purification of T109S mutant DHOase.

### 2.2. Crystallization

Purification procedures for T109S DHOase were adapted from the previous report for wild-type DHOase (Washabaugh & Collins, 1984). The purified protein was dialyzed into 20 m$M$ Na HEPES pH 7.2 and 1 m$M$ DTT. Crystals were grown by the hanging-drop vapour-diffusion method at 277 K. In the initial attempt to grow crystals of T109S DHOase, the crystallization conditions for native DHOase were applied, using 2 µl protein solution (8.2 mg ml$^{-1}$) mixed with 2 µl reservoir solution (15–20% PEG 3350, 0.1 $M$ MES pH 6–6.5, 75 m$M$ MgCl$_2$ and 0.15 $M$ KCl) and 0.45 µl 100 m$M$ L-DHO (Lee *et al.*, 2005). Crystallization conditions were modified slightly in order to increase the stability of tetragonal crystals by using reservoir solution containing 14–16% PEG 3350, 0.1 $M$ MES pH 6.25, 25 m$M$ MgCl$_2$,
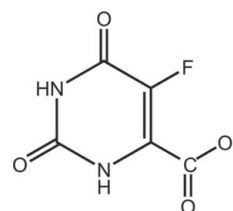


**Figure 2**
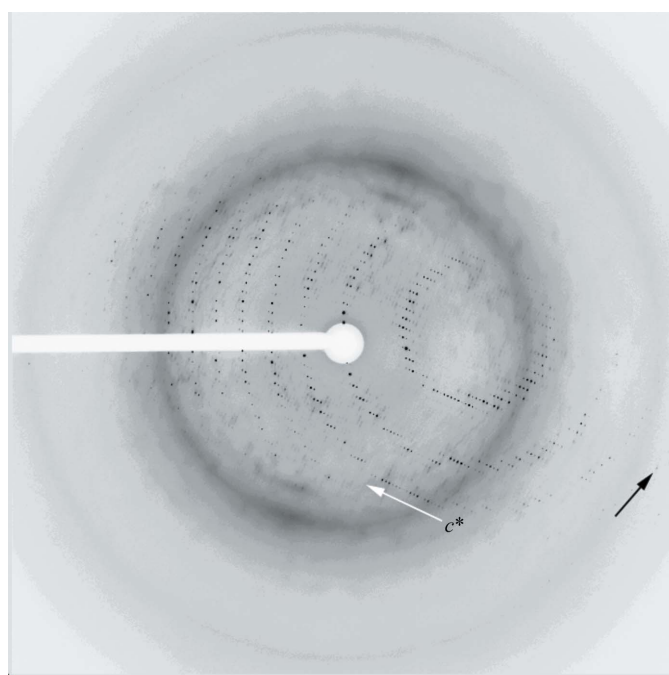Structure of 5-fluoroorotate (FOA).

**Table 1**
Statistics of the data collection and refinement.

Values in parentheses are for the outer shell.

| | |
|---|---|
| X-ray source | APS 23-ID |
| Wavelength (Å) | 0.9793 |
| Space group | $P4_12_12$ |
| Unit-cell parameters (Å) | $a = b = 72.6$, $c = 176.1$ |
| Resolution ($a*$, $b*$, $c*$ directions)† (Å) | 3.0, 3.0, 2.7 |
| Mosaicity (°) | 0.5 |
| No. of unique reflections | 10367 |
| Completeness‡ (%) | 75.8 (29.9) |
| Redundancy | 6.7 (5.9) |
| $R_{merge}$ (%) | 2.3 (8.7) |
| Average $I/\sigma(I)$ | 20.5 (1.9) |
| $R_{work}$ | 0.218 (0.187) |
| $R_{free}$ | 0.257 (0.234) |
| No. of reflections in test set | 490 [4.7%] |
| Protein atoms (including Zn) | 2689 |
| Heteroatoms§ | 12 |
| Water molecules | 10 |
| R.m.s.d. bond lengths (Å) | 0.01 |
| R.m.s.d. angles (°) | 0.93 |
| Mean protein $B$ factor, all non-H atoms (Å$^2$) | 63.0 |
| Estimated standard uncertainties¶ (Å) | 0.27 |
| Ramanchandran plot, residues in†† | |
| Most favoured regions (%) | 87.6 |
| Additional allowed regions (%) | 11.7 |
| Generously allowed regions (%) | 0.7 |

† Because of the severe diffraction anisotropy, data beyond these limits were excluded during refinement. ‡ Completeness was calculated using the entire spherical shell of resolution 2.7 Å. § One FOA molecule. ¶ Estimated standard uncertainty in atomic position, based on maximum likelihood (Murshudov *et al.*, 1997). †† Calculated using *PROCHECK* (Laskowski *et al.*, 1993).

0.2 *M* KCl and 30% sucrose. 10 m*M* 5-fluoroorotate (FOA, Sigma) was added to the drop to replace L-DHO. Crystals typically grew overnight. Prior to data collection, the crystals were further cryo-protected by adding 2 µl reservoir solution to the drop and were flash-cooled in a stream of nitrogen gas at 100 K.



**Figure 3**
Diffraction pattern from a tetragonal crystal of *E. coli* T109S DHOase recorded on beamline 23-ID at APS. The diffraction is severely anisotropic; reflections are observed along $c*$ (indicated by the white arrow) to 2.2 Å (black arrow). The resolution at the edge of the image belonging to 2.13 Å.

## 2.3. Data collection and processing

Synchrotron data were recorded to 2.2 Å resolution from a single crystal on beamline 23-ID at the Advanced Photon Source (APS), Argonne National Laboratory using a MAR mosaic 300 CCD detector (MAR USA) with a wavelength of 0.9793 Å at 100 K. A total of 190 successive frames were collected with an oscillation angle of 0.5°, giving a total coverage of 95° and an overall redundancy of 6.1. The diffraction data were processed and scaled with *HKL*-2000 (Otwinowski & Minor, 1997). The unit-cell parameters are $a = b = 72.6$, $c = 176.1$ Å, $\alpha = \beta = \gamma = 90°$. The data could be processed in either space group *P*4 or *P*422 with similar results ($R_{merge} = 0.040$ in *P*4, 0.043 in *P*422). The higher-symmetry Laue group was preferred and chosen for molecular replacement and was subsequently confirmed by the structure refinement. The Matthews coefficient for space group *P*422 ($V_M = 3.0$ Å$^3$ Da$^{-1}$) suggests there is one monomer per asymmetric unit, with a calculated solvent content of 58.9% (Matthews, 1968).
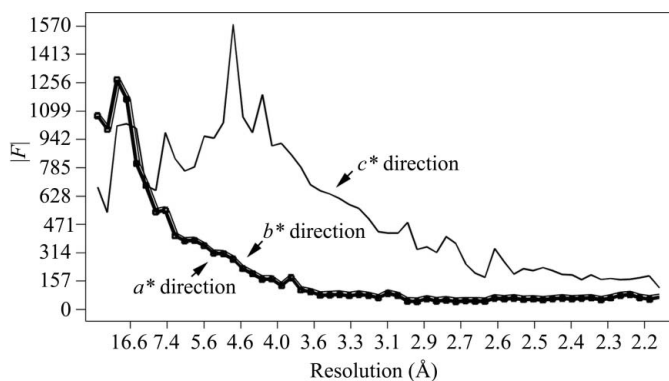
## 2.4. Structure solution and refinement

Despite the fact that reflections were clearly visible in diffraction images to a resolution of 2.2 Å, the inherent anisotropy of the diffraction resulted in a severe limitation in the completeness of the data beyond 2.7 Å resolution (Fig. 3 and Table 1). Therefore, only data to 2.7 Å were used for structure solution and refinement.

The crystal structure was solved by molecular replacement using *Phaser* from the *CCP*4 suite (Collaborative Computational Project, Number 4, 1994; Storoni *et al.*, 2004). Chain *A* of the native DHOase structure in space group $P2_12_12_1$ (PDB code 1xge; Lee *et al.*, 2005) was used as the search model. The Zn atoms, ligand molecule and solvent molecules were deleted from the search model. Residues 105–115 were given zero occupancy to avoid model bias in the phase calculation.

The fast rotation function of *Phaser* found one significant solution, which was then used for fast translation searches in all eight possible space groups *P*422, $P42_12$, $P4_122$, $P4_12_12$, $P4_222$, $P4_22_12$, $P4_322$ and $P4_32_12$. The best solution was found in $P4_12_12$; the *Z* score and the log-likelihood gain (LLG) increased from 8.6 to 36.5 and from 115 to 863, respectively, after the fast translation function.

Structure refinement was carried out using *REFMAC*5 (Collaborative Computational Project, Number 4, 1994; Murshudov *et al.*, 1997). 4.7% of the reflections were randomly selected to create an independent data set of test reflections for cross-validation throughout the refinement procedure. The initial attempt to refine the structure using the data set to 2.7 Å resulted in atomic coordi-



**Figure 4**
Analysis of the anisotropy of the data calculated using the program *TRUNCATE* (French & Wilson, 1978).

**Table 2**
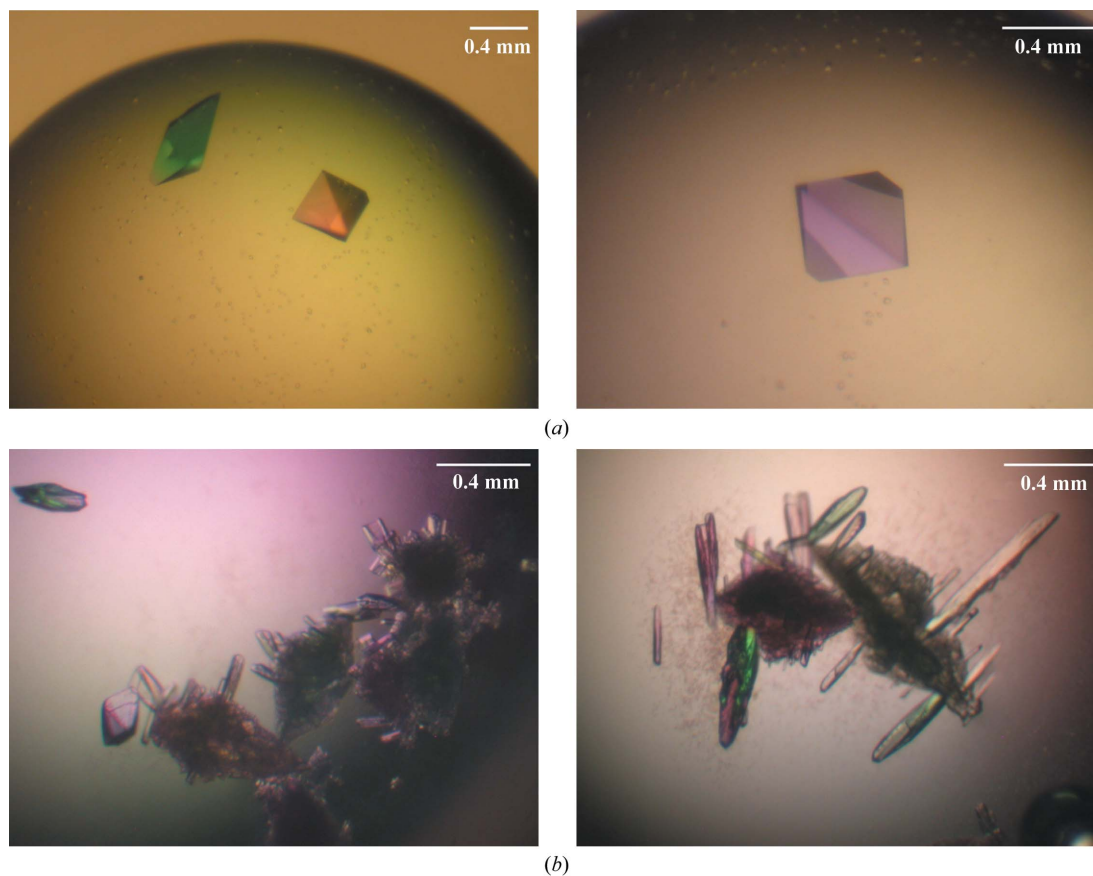Completeness statistics of pre- and post-anisotropy correction of diffraction data.

Completeness was calculated using the entire spherical shell. The anisotropy correction removes all reflections lying outside the defined ellipsoid. The completeness measured as a percentage of the spherical shell is therefore lower following the correction. Data beyond a resolution of 2.7 Å were not used in the refinement (see Table 1).

| | | Before correction | | After correction | |
|---|---|---|---|---|---|
| Resolution | Expected No. of reflections | Observed No. of reflections | % observed | Observed No. of reflections | % observed |
| 31.00–5.97 | 1397 | 1343 | 96.1 | 1338 | 95.8 |
| 5.97–4.74 | 1299 | 1279 | 98.5 | 1274 | 98.1 |
| 4.74–4.14 | 1274 | 1222 | 95.9 | 1215 | 95.4 |
| 4.14–3.76 | 1257 | 1211 | 96.3 | 1190 | 94.7 |
| 3.76–3.49 | 1249 | 1221 | 97.8 | 1210 | 96.9 |
| 3.49–3.29 | 1226 | 1162 | 94.8 | 1167 | 95.2 |
| 3.29–3.12 | 1246 | 1112 | 89.2 | 999 | 80.2 |
| 3.12–2.99 | 1238 | 872 | 70.4 | 668 | 54.0 |
| 2.99–2.87 | 1226 | 683 | 55.7 | 536 | 43.7 |
| 2.87–2.77 | 1229 | 618 | 50.3 | 434 | 35.3 |
| 2.77–2.69 | 1209 | 540 | 44.7 | 339 | 28.0 |
| 2.69–2.61 | 1225 | 516 | 42.1 | 287 | 23.4 |
| 2.61–2.54 | 1220 | 481 | 39.4 | 237 | 19.4 |
| 2.54–2.48 | 1221 | 418 | 34.2 | 187 | 15.3 |
| 2.48–2.42 | 1197 | 461 | 38.5 | 164 | 13.7 |
| 2.42–2.37 | 1218 | 504 | 41.4 | 123 | 10.1 |
| 2.37–2.32 | 1198 | 462 | 38.6 | 94 | 7.8 |
| 2.32–2.28 | 1212 | 520 | 42.9 | 73 | 6.0 |
| 2.28–2.24 | 1207 | 458 | 37.9 | 52 | 4.3 |
| 2.24–2.20 | 1208 | 462 | 38.2 | 30 | 2.5 |
| Overall | 24756 | 15545 | 62.8 | 11617 | 46.9 |

reflections along the $a*$ and $b*$ directions by using a spherical resolution limit impeded the refinement. We utilized the diffraction-anisotropy server (http://nihserver.mbi.ucla.edu/anisoscale; Strong *et al.*, 2006) to analyse the data. The recommended resolution limits along $a*$, $b*$, and $c*$ were 3.0, 3.0 and 2.2 Å, respectively, as indicated by the program *TRUNCATE* (Table 2 and Fig. 4; French & Wilson, 1978). Reflections falling outside the ellipsoid defined by the specified resolutions were discarded and the remaining data were scaled with anisotropic parameters (Lodowski *et al.*, 2003; Zhang *et al.*, 2004). A negative isotropic *B*-factor correction was applied to restore the magnitude of the high-resolution reflections that was diminished by anisotropic scaling. This anisotropy-corrected data set provided by the diffraction-anisotropy server was used for further refinement using *REFMAC*5. Several rounds of rigid-body refinement for data in the resolution range 31–3.0 Å gave $R = 0.36$ and $R_{free} = 0.36$. The model was then subjected to restrained refinement using TLS (Winn *et al.*, 2001) with data to 2.7 Å. The initial difference Fourier maps clearly showed that the surface loop (residues 105–115), omitted from the model, was in the 'loop-out' conformation. Further refinement with *REFMAC*5 was interspersed with manual model building using *Coot* (Emsley & Cowtan, 2004). In the final stages of the refinement, the FOA inhibitor was modelled into difference electron density in the active site and refined. The FOA parameters were generated with the assistance of the *PRODRG* server (Schüttelkopf & van Aalten, 2004).

Model validation was conducted using *PROCHECK* (Laskowski *et al.*, 1993), *WHAT-CHECK* (Hooft *et al.*, 1996) and the *MOLPROBITY* server (Lovell *et al.*, 2003). *PROCHECK* reported

nates with high *B* factors (over 100 Å$^2$). Since the data were severely anisotropic, we reasoned that the inclusion of unmeasurably weak



(a)



(b)

**Figure 5**
Crystals of *E. coli* T109S DHOase. Tetragonal crystals belonging to space group $P4_12_12$ (a) are very unstable and often disintegrated shortly after crystal formation (b). The small crystals grown around the remnants of the tetragonal crystals are orthorhombic crystals belonging to space group $P2_12_12_1$.

that 87.6% of the residues fell in the most favoured region of the Ramachandran plot and 11.7% of the residues were in additionally allowed regions. Two residues (His177 and Arg20) were found in the generously allowed regions. This observation is consistent with that from the high-resolution wild-type structure. Superposition and calculation of root-mean-square differences were performed using the program *LSQMAN* (Kleywegt & Jones, 1997). Figures were generated using *PyMOL* (DeLano Scientific, San Carlos, CA, USA).
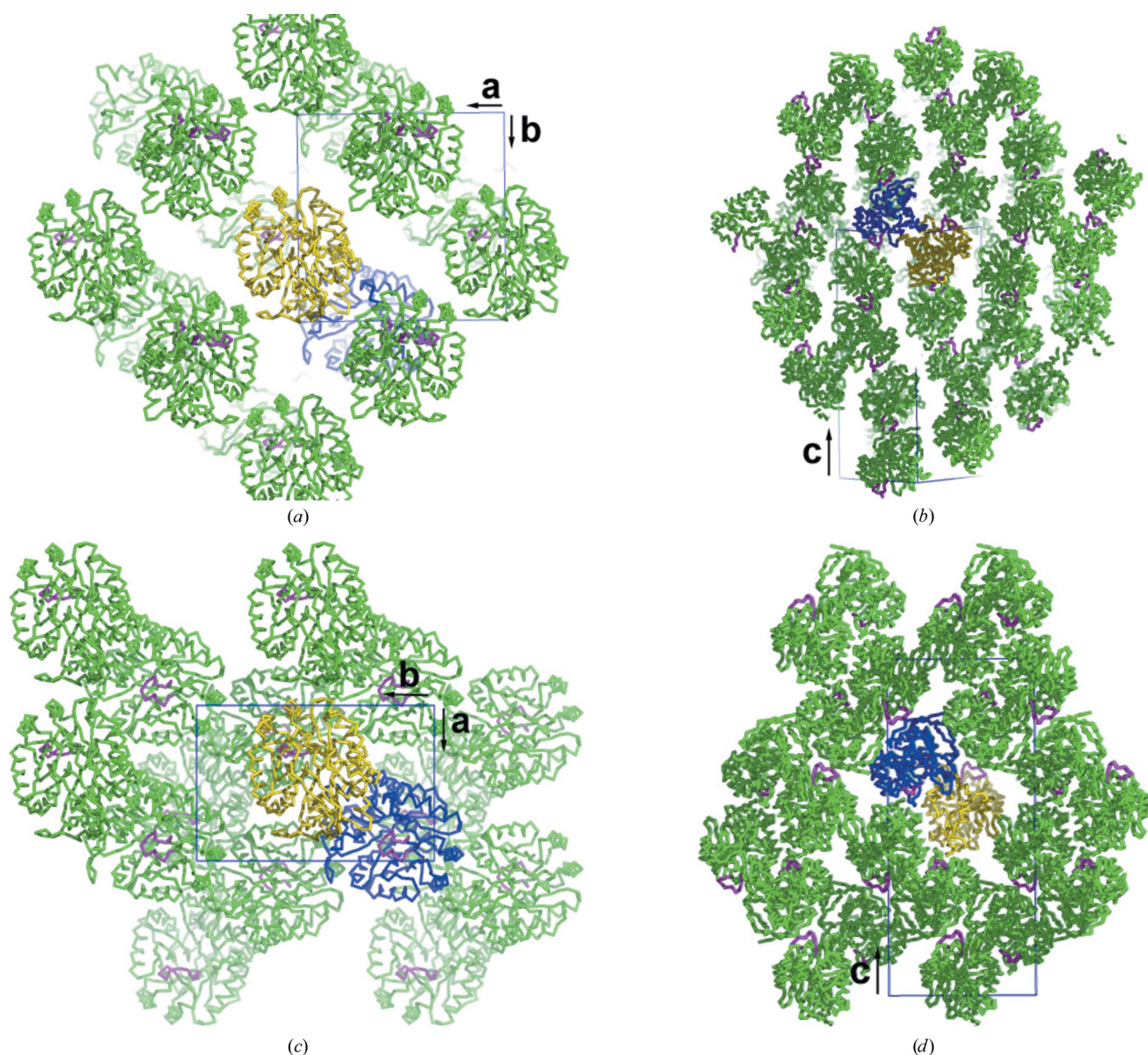
## 3. Results and discussion

### 3.1. Crystal instability

The initial attempt to grow crystals of T109S DHOase in the presence of L-DHO using the crystallization conditions for wild-type crystals unexpectedly produced tetragonal crystals rather than the orthorhombic crystals characteristic of the wild-type enzyme. However, these crystals, which grew in 24 h, were extremely unstable and disintegrated shortly after formation (Fig. 5). Diffraction from these short-lived crystals was too poor to record diffraction data for refinement. However, the space group and unit-cell parameters could be determined unambiguously and were found to be identical to those of the FOA complex of T109S DHOase reported in this paper. Orthorhombic crystals isomorphous to those of the wild-type DHOase subsequently grew from the debris of the tetragonal crystals or at new nucleation sites in the same drops.

Attempts to stabilize the tetragonal crystals in the presence of L-DHO by varying the conditions failed. We reasoned that the crystal instability was caused when catalysis had generated sufficient L-CA-asp to bind to the DHOase, resulting in a movement of the flexible loop (residues 105–115). Evidence for this hypothesis was ultimately
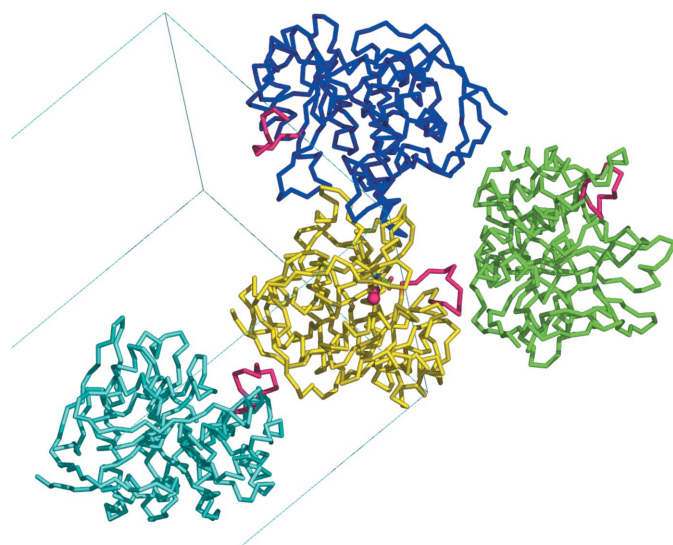


**Figure 6**
DHOase crystal packing. (*a*, *b*) Tetragonal FOA complex of T109S DHOase. The monomer in the asymmetric unit is shown in yellow, with the flexible surface loops (residues 105–115) in magenta. The other monomer of the dimer is shown in blue. Other symmetry-related dimers are shown in green. (*c*, *d*) Crystal packing of the orthorhombic wild-type DHOase. Chain *A* with the 'loop-out' conformation is shown in yellow and chain *B* with the 'loop-in' conformation in blue. The projection is down along the *c* axis in (*a*) and (*c*) and perpendicular to the *c* axis in (*b*) and (*d*).

obtained by analysis of the tetragonal crystal structure (see §3.4). To stabilize the tetragonal crystals, we used FOA, a product mimic, for crystallization in place of L-DHO (Fig. 2). Since FOA cannot be hydrolysed by the enzyme, the formation of a symmetrical dimer with FOA in both active sites was possible. The crystals grown in the presence of FOA were stable and data were successfully collected. The diffraction from the crystals was very anisotropic. Reflections were observable to 2.2 Å resolution parallel to $c*$ but only to about 3 Å perpendicular to this direction (Figs. 3 and 4).

The structure was solved by molecular replacement and refined to 2.7 Å resolution in space group $P4_12_12$ with a monomer in the asymmetric unit (Table 1).

## 3.2. Description of the structure

The final model consists of one monomer of *E. coli* T109S DHOase with 343 protein residues, ten water molecules, two Zn atoms and one molecule of FOA. Refinement using *REFMAC*5 with TLS converged with residuals $R = 0.218$ and $R_{free} = 0.257$. Anisotropy correction of the diffraction data and the use of the TLS parameters in refinement improved the electron-density maps and refinement statistics. The molecular structure of *E. coli* T109S DHOase in space group $P4_12_12$ is closely similar to the previously solved wild-type structure in space group $P2_12_12_1$ [PDB codes 1j79 (Thoden *et al.*, 2001) and 1xge (Lee *et al.*, 2005)]. The crystals of both forms were grown under similar conditions, except for the addition of sucrose to the tetragonal crystallization conditions to provide further stabilization and cryoprotection. The core of the molecule forms a TIM-barrel fold with eight alternating $\beta$-strands/$\alpha$-helices. Crystals of the wild-type enzyme in space group $P2_12_12_1$ have a dimer in the asymmetric unit, while those of T109S DHOase in space group $P4_12_12$ have only a monomer. There are no significant differences between the main-chain $C^\alpha$ positions of chain *A* from the wild-type structure and the mutant structure; the overall difference in r.m.s. distance for 343 residues is 0.23 Å, which is within the ESU of the mutant structure (0.27 Å; Murshudov *et al.*, 1997). Apart from the residues at the

**Table 3**
Crystal contacts between symmetry-related molecules in the tetragonal T109S crystal.

Space group $P4_12_12$; PDB code 2e25. Dimer-interface interactions were not considered.

| Atom X | Atom Y | Distance† (Å) | Symmetry operation‡ |
|---|---|---|---|
| Lys8 N$^\zeta$ | Ser83 O | 3.0 | i |
| Arg10 N$^{\eta2}$ | Asp82 O$^{\delta2}$ | 2.7 | i |
| Glu292 O$^{\varepsilon1}$ | Ser112 N | 2.7 | i |
| Glu292 O$^{\varepsilon2}$ | Ser112 O$^\gamma$ | 2.8 | i |
| Asp82 O$^{\delta2}$ | Arg10 N$^{\eta2}$ | 2.7 | ii |
| Ser83 O | Lys8 N$^\zeta$ | 3.0 | ii |
| Ser112 N | Glu292 O$^{\varepsilon1}$ | 2.7 | ii |
| Ser112 O$^\gamma$ | Glu292 O$^{\varepsilon2}$ | 2.8 | ii |

† All interactions from 2.5 to 3.3 Å between potential hydrogen-bond donors and acceptors are included.  ‡ (i) $-y + 1/2, x + 1/2, z + 1/4$; (ii) $y - 1/2, -x + 1/2, z - 1/4$.

termini, the largest difference (0.64 Å) between chain *A* of the wild-type structure and the mutant structure is the mutated residue Ser109 (Thr in the native structure). In contrast, superposition of chain *B* of the wild-type structure with the mutant structure gives an r.m.s. difference of $C^\alpha$ positions of 1.65 Å, with the greatest distance between pairs of $C^\alpha$ atoms being 14.0 Å for the same mutated residue, Ser109. In the wild-type structure the flexible loops (residues 105–115) are in different conformations: 'out' when L-DHO is in the active site (chain *A*) and 'in' when L-CA-asp is in the active site (chain *B*). In the tetragonal crystal forms the two monomers in the dimer are crystallographically identical and the loop adopts the 'out' conformation in both, consistent with the presence of a product mimic, FOA, in both active sites.

## 3.3. Analysis of the crystal contacts

Analysis of the contacts between the symmetry-related molecules in the crystals provides support for the hypothesis that loop movement, catalysis and crystal packing are linked. Despite the fact that the solvent content of the tetragonal crystals is within the typical range for a protein the size of DHOase (58.9%), the molecules in the crystals make very few contacts (Figs. 6 and 7). The crystal contacts occur predominantly along the *c* axis, explaining the severe anisotropy of the diffraction. There are only three symmetry-related molecules that make direct contacts and one of them is the other monomer of the dimer ($y, x, -z$) (Fig. 7). The other two molecules ($y - 1/2, -x + 1/2, z - 1/4; -y + 1/2, x + 1/2, z + 1/4$) make equivalent contacts *via* only four hydrogen bonds. Of these four hydrogen bonds, two involve Ser112 in the flexible surface loop (residues 105–115; Fig. 8; Table 3). Ser112 forms two hydrogen bonds with Glu*292 in a symmetry-related molecule ($y - 1/2, -x + 1/2, z - 1/4$) (Ser112 N···Glu*292 O$^{\varepsilon1}$, 2.7 Å; Ser112 O$^\gamma$···Glu292 O$^{\varepsilon2}$, 2.8 Å). Residues Asp82 and Ser83 are involved in the other two hydrogen bonds with residues Arg*10 and Lys*8 from the same symmetry-related molecule ($y - 1/2, -x + 1/2, z - 1/4$) (Asp82 O$^{\delta2}$···Arg*10 N$^{\eta2}$, 2.7 Å; Ser83 O···Lys*8 N$^\zeta$, 3.0 Å). The equivalent set of interactions with the residues Lys8, Arg10 and Glu292 are observed in interactions with the second symmetry-related molecule ($-y + 1/2, x + 1/2, z + 1/4$). Therefore, the packing of molecules in this crystal form depends on residues in the flexible surface loop (residues 105–115).

Superposition of the 'loop-in' conformation from the wild-type structure (chain *B* from 1xge) onto the tetragonal structure clearly illustrates the effect of the movement of the loop (Fig. 8*b*) on the crystal contacts. If the flexible loop moves in towards the active site, the two hydrogen bonds involving Ser112 will be lost. The loss of these contacts is apparently sufficient to destabilize the crystal

# protein structure communications

**Table 4**
Crystal contacts between symmetry-related molecules in the orthorhombic wild-type crystal.

Space group $P2_12_12_1$; PDB code 1xge.

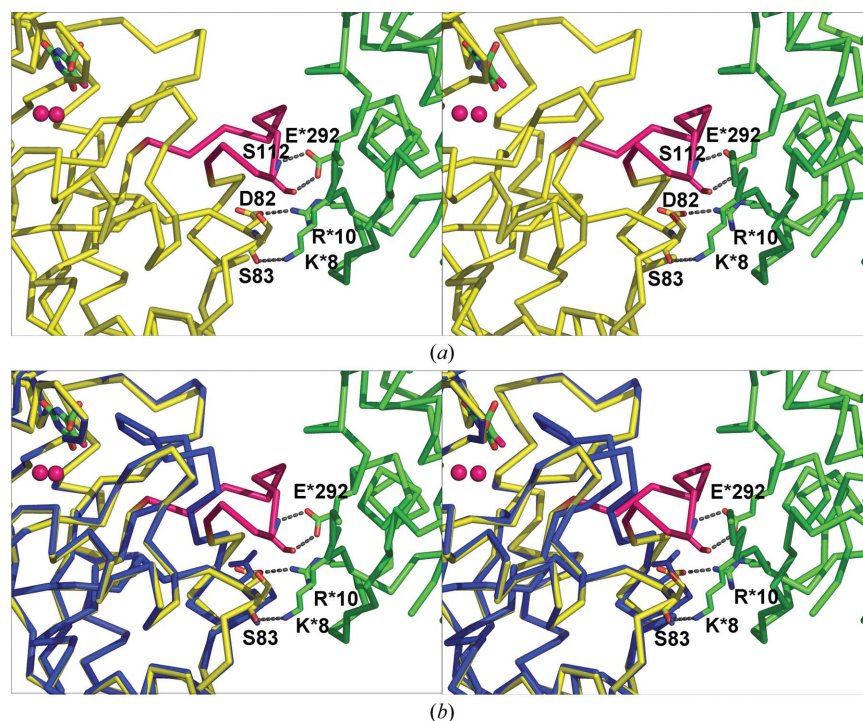| Atom X | Atom Y | Distance† (Å) | Symmetry operation‡ |
|---|---|---|---|
| **Chain A** | | | |
| LysA8 N$^\zeta$ | AlaB121 O | 2.8 | i |
| ArgA10 N$^{\eta 2}$ | AspB120 O$^{\delta 2}$ | 3.1 | i |
| GlyA6 N | AsnB94 O | 3.0 | ii |
| AsnA94 O | GlyB69 N | 3.0 | iii |
| AspA82 O$^{\delta 2}$ | ArgB10 N$^{\eta 2}$ | 2.9 | iv |
| SerA83 O | LysB8 N$^\zeta$ | 2.8 | iv |
| SerA112 N | GluB292 O$^{\varepsilon 1}$ | 2.8 | iv |
| SerA112 O$^\gamma$ | GluB292 O$^{\varepsilon 2}$ | 2.7 | iv |
| GluA130 O$^{\varepsilon 1}$ | ArgB256 N$^{\eta 1}$ | 3.3 | v |
| LysA131 N$^\zeta$ | LeuB327 O | 2.7 | v |
| ArgA256 N$^{\eta 1}$ | GluB130 O$^{\varepsilon 1}$ | 3.3 | vi |
| LeuA327 O | LysB131 N$^\zeta$ | 2.7 | vi |
| **Chain B** | | | |
| LysB8 N$^\zeta$ | SerA83 O | 2.8 | I |
| ArgB10 N$^{\eta 2}$ | AspA82 O$^{\delta 2}$ | 2.9 | I |
| GluB292 O$^{\varepsilon 1}$ | SerA112 N | 2.8 | I |
| GluB292 O$^{\varepsilon 2}$ | SerA112 O$^\gamma$ | 2.7 | I |
| AspB82 O | LysA8 N$^\zeta$ | 3.0 | II |
| AspB120 O$^{\delta 2}$ | ArgA10 N$^{\eta 2}$ | 3.1 | II |
| AlaB121 O | LysA8 N$^\zeta$ | 2.8 | II |
| ArgB91 N$^\varepsilon$ | GluB317 O$^{\varepsilon 1}$ | 3.3 | III |
| ArgB91 N$^{\eta 1}$ | GluB317 O$^{\varepsilon 2}$ | 2.8 | III |
| ArgB91 N$^{\eta 2}$ | GluB317 O$^{\varepsilon 1}$ | 3.2 | III |
| AsnB94 O | GlnB319 O$^{\varepsilon 1}$ | 3.3 | III |
| GluB317 O$^{\varepsilon 1}$ | ArgB91 N$^\varepsilon$ | 3.3 | IV |
| GluB317 O$^{\varepsilon 1}$ | ArgB91 N$^{\eta 2}$ | 3.2 | IV |
| GluB317 O$^{\varepsilon 2}$ | ArgB91 N$^{\eta 1}$ | 2.8 | IV |
| GlnB319 O$^{\varepsilon 1}$ | AsnB94 O | 3.3 | IV |

† All interactions from 2.5 to 3.3 Å between potential hydrogen-bond donors and acceptors are included.   ‡ (i) $x + 1/2, -y + 1/2, -z + 1$; (ii) $x - 1/2, -y + 3/2, 1 - z$; (iii) $x + 1/2, -y + 3/2, -z + 1$; (iv) $-x + 1, y + 1/2, -z + 1/2$; (v) $x + 1, y, z$; (vi) $x - 1, y, z$; (I) $-x + 1, y - 1/2, -z + 1$; (II) $x - 1/2, -y + 1/2, -z + 1$; (III) $-x, y - 1/2, -z + 1/2$; (IV) $-x, y + 1/2, -z + 1/2$.

packing. Therefore, the packing of molecules in this crystal form can only be maintained when the loop is in the 'out' conformation. The presence of a product mimic, FOA, in both active sites is incompatible with the 'loop-in' conformation and it is therefore able to stabilize the tetragonal crystals, which require both loops to be 'out'.

Unlike in the tetragonal crystal, where the crystal contacts made by only two regions of the structure are responsible for the stability of the crystal packing, the molecules in the wild-type orthorhombic form make many more crystal contacts (Fig. 6 and Table 4). The chain A molecule in the orthorhombic crystals, which has the 'loop-out' conformation, makes 12 hydrogen-bond interactions with six different symmetry-related molecules. Interestingly, these include the same crystal contact that is observed in tetragonal crystals in which residues Asp82, Ser83 and Ser112 interact with residues Lys*8, Arg*10 and Glu*292 of a symmetry-related molecule. In the orthorhombic crystals, in which the two chains have different conformations, the equivalent hydrogen-bonded contacts involving residues on chain B are incompatible with the 'loop-in' conformation. The chain B molecule in the orthorhombic crystal makes other crystal contacts with four different symmetry-related molecules via 14 hydrogen-bonding interactions. Each dimer in the orthorhombic crystals makes direct contacts with a total of ten symmetry-related molecules, whereas the equivalent dimers (two monomers) in the tetragonal crystals make direct contacts with only four symmetry-related molecules.

### 3.4. Conformational change of DHOase and crystal formation

The combination of few contacts between molecules in the crystal and the involvement of the flexible loop (residues 105–115) in the crystal packing explains the instability of this crystal form when the protein was crystallized in the presence of L-DHO. Thr109 is one of



**Figure 8**
Crystal contacts between symmetry-related molecules in the tetragonal FOA complex of T109S DHOase. The symmetry-related molecule ($y − 1/2, −x + 1/2, z − 1/4$) is coloured green. The flexible loop (residues 105–115) is shown in magenta. The Zn atoms and FOA molecule are displayed in the active site. (a) shows the hydrogen bonds involved between the two molecules. (b) displays the superposition of the 'loop-in' conformation from the wild-type structure (chain B from PDB code 1xge, blue) onto the tetragonal structure.

two threonine residues (Thr109 and Thr110) that are directly involved in the hydrogen-bonding interactions between the surface loop (residues 105–115) and the bound substrate L-CA-asp in the active site in the structure of wild-type *E. coli* DHOase (Lee *et al.*, 2005). Mutation of this residue to serine reduces the catalytic activity of *E. coli* DHOase to about 30% of that of the wild-type enzyme[1]. Despite the conservative nature of the mutation, Ser for Thr, we presume that the decreased activity results from the greater conformational flexibility of the Ser side chain, which destabilizes the interaction with the substrate. As a result of the lower activity, the conversion of L-DHO to L-CA-asp is slower and initially allows a high population of DHOase with L-DHO in both active sites and both loops in the 'out' conformation. This permits the protein to crystallize in the tetragonal form with the loops of each monomer involved in crystal contacts. As L-DHO is slowly converted to L-CA-asp, the flexible loop moves in to close the active site, breaking the crystal contacts stabilized by the loop in its 'out' conformation, which then results in the disintegration of the crystals. Once sufficient L-CA-asp is available, dimers with L-CA-asp in one subunit and L-DHO in the other can form and orthorhombic crystals can grow. Wild-type enzyme converts L-DHO to L-CA-asp sufficiently rapidly that there is never a sufficient population of enzyme with L-DHO bound to both subunits to produce the tetragonal crystals.

## 4. Conclusions

We have observed the progress of the enzymatic reaction of DHOase by the formation of one crystal form in the presence of L-DHO, its subsequent dissolution as a loop moves during catalysis and the ultimate formation of a new crystal form with both substrate and product bound. The complex with L-DHO bound in both subunits could only be visualized as an inhibitor complex of *E. coli* T109S DHOase with lower activity. The surface loop that moves during catalysis plays a crucial role in anchoring symmetry-related molecules together in the tetragonal crystals. This explains the instability of the tetragonal crystals when crystallized in the presence of L-DHO rather than the nonhydrolysable analogue FOA.

## References

Brown, D. C. & Collins, K. D. (1991). *J. Biol. Chem.* **266**, 1597–1604.
Christopherson, R. I. & Jones, M. E. (1979). *J. Biol. Chem.* **254**, 12506–12512.
Collaborative Computational Project, Number 4 (1994). *Acta Cryst.* D**50**, 760–763.
Emsley, P. & Cowtan, K. (2004). *Acta Cryst.* D**60**, 2126–2132.
Fields, C., Brichta, D., Shepherdson, M., Farinha, M. & O'Donovan, G. (1999). *Paths Pyrimidines*, **7**, 49–63.
French, S. & Wilson, K. (1978). *Acta Cryst.* A**34**, 517–525.
Gutteridge, A. & Thornton, J. (2004). *FEBS Lett.* **567**, 67–73.
Hammes, G. G. (2002). *Biochemistry*, **41**, 8221–8228.
Holm, L. & Sander, C. (1997). *Proteins*, **28**, 72–82.
Hooft, R. W. W., Vriend, G., Sander, C. & Abola, E. E. (1996). *Nature (London)*, **381**, 272.
Kempner, E. S. (1993). *FEBS Lett.* **326**, 4–10.
Kleywegt, G. J. & Jones, T. A. (1997). *Methods Enzymol.* **277**, 525–545.
Laskowski, R. A., MacArthur, M. W., Moss, D. S. & Thornton, J. M. (1993). *J. Appl. Cryst.* **26**, 283–291.
Lee, M., Chan, C. W., Guss, J. M., Christopherson, R. I. & Maher, M. J. (2005). *J. Mol. Biol.* **348**, 523–533.
Lodowski, D. T., Pitcher, J. A., Capel, W. D., Lefkowitz, R. J. & Tesmer, J. J. (2003). *Science*, **300**, 1256–1262.
Lovell, S. C., Davis, I. W., Arendall, W. B. III, de Bakker, P. I., Word, J. M., Prisant, M. G., Richardson, J. S. & Richardson, D. C. (2003). *Proteins*, **50**, 437–450.
Martin, P. D., Purcarea, C., Zhang, P., Vaishnav, A., Sadecki, S., Guy-Evans, H. I., Evans, D. R. & Edwards, B. F. (2005). *J. Mol. Biol.* **348**, 535–547.
Matthews, B. W. (1968). *J. Mol. Biol.* **33**, 491–497.
Murshudov, G. N., Vagin, A. A. & Dodson, E. J. (1997). *Acta Cryst.* D**53**, 240–255.
Otwinowski, Z. & Minor, W. (1997). *Methods Enzymol.* **276**, 307–326.
Porter, T. N., Li, Y. & Raushel, F. M. (2004). *Biochemistry*, **43**, 16285–16292.
Sander, E. G., Wright, L. D. & McCormick, D. B. (1965). *J. Biol. Chem.* **240**, 3628–3630.
Schüttelkopf, A. W. & van Aalten, D. M. (2004). *Acta Cryst.* D**60**, 1355–1363.
Simmer, J. P., Kelly, R. E., Rinker, A. G. Jr, Zimmermann, B. H., Scully, J. L., Kim, H. & Evans, D. R. (1990). *Proc. Natl Acad. Sci. USA*, **87**, 174–178.
Storoni, L. C., McCoy, A. J. & Read, R. J. (2004). *Acta Cryst.* D**60**, 432–438.
Strong, M., Sawaya, M. R., Wang, S., Phillips, M., Cascio, D. & Eisenberg, D. (2006). *Proc. Natl Acad. Sci. USA*, **103**, 8060–8065.
Thoden, J. B., Phillips, G. N. Jr, Neal, T. M., Raushel, F. M. & Holden, H. M. (2001). *Biochemistry*, **40**, 6989–6997.
Washabaugh, M. W. & Collins, K. D. (1984). *J. Biol. Chem.* **259**, 3293–3298.
Washabaugh, M. W. & Collins, K. D. (1986). *J. Biol. Chem.* **261**, 5920–5929.
Williams, N. K., Simpson, R. J., Moritz, R. L., Peide, Y., Crofts, L., Minasian, E., Leach, S. J., Wake, R. G. & Christopherson, R. I. (1990). *Gene*, **94**, 283–288.
Winn, M. D., Isupov, M. N. & Murshudov, G. N. (2001). *Acta Cryst.* D**57**, 122–133.
Zhang, M., Monzingo, A. F., Segatori, L., Georgiou, G. & Robertus, J. D. (2004). *Acta Cryst.* D**60**, 1512–1518.

[1] The relative enzyme activity was measured by direct spectrophotometric assay at 230 nm (Sander *et al.*, 1965). The linear increase in absorbance at 230 nm arising from the formation of L-DHO ($\varepsilon_{230} = 1.17$ m$M^{-1}$ cm$^{-1}$) was measured and the initial reaction rates were calculated.